

Original Research Article**Effect of temperature on Structural, Magnetic and Dielectric Properties of Cobalt ferrite Nanoparticles Prepared via Co-precipitation Method****Abstract**

Nano-crystalline cobalt ferrite powders have been synthesized by coprecipitation method and characterized to investigate the effect of thermal treatment on the structural, dielectric, and magnetic properties of the prepared sample. The structural/morphological, dielectric, and magnetic properties of the products were determined by X-ray diffraction (XRD), transmission electron microscopy (TEM), open ended coaxial probe and vibrating sample magnetometer (VSM). Results from analysis confirm that thermal heat influences the magnitude of magnetization, dielectric and surface morphology of samples. The variation of dielectric properties with frequency reveals that the variation in magnitude is due to Maxwell–Wagner type of interfacial polarization as well as hopping of charge from Fe^{2+} to Fe^{3+} and from Co^{2+} to Co^{3+} ions at B-sites.

Keywords: nanoparticles, ferrites, spinel, cobalt ferrite, permittivity

Introduction

Magnetic nanostructured materials have gained great interest of the scientists due to their unusual physical properties compared to their bulk form. They have very large areas of applications in technology, such as electronic devices, microwave devices, transformer cores, magnetic devices, switching devices, recording tapes, permanent magnets, hard disc recording media, flexible recording media, read–write heads, active components of ferrofluids, magnetic drug delivery, catalysis, color imaging, magnetic refrigeration, detoxification of biological fluids, magnetically controlled transport of anti-cancer drugs, magnetic resonance imaging (MRI) contrast enhancement and magnetic cell

TO REMOVE SPACE

27 separation [1].

28 The ferrite nanoparticles have a spinel structure and the general spinel structure is in the form as
29 AB_2O_4 . Cobalt ferrite is a partially inverted spinel structure with cobalt atoms predominantly in the
30 octahedral sites [2] and it is a well-known hard magnetic material, which has been studied in detail due
31 to its high coercivity (5400 Oe), high chemical stability, good electrical insulation, significant
32 mechanical hardness and moderate saturation magnetization (80 emu/g) at room temperature.

33 Nanoferrites are simultaneously good magnetic and dielectric materials. These properties of the ferrites
34 are governed by the choice of the cations and their distribution between tetrahedral and octahedral sites
35 of the spinel lattice. The properties of the nanoferrites are also affected by the preparation conditions,
36 chemical composition, sintering temperature, doping additives, and the method of preparation [3].

37 Several chemical and physical methods such as spray pyrolysis, sol-gel, coprecipitation, combustion
38 technique, high energy milling, and so forth have been used for the fabrication of stoichiometric and
39 chemically pure nanoferrite materials [4]. Among the available synthesis methods, solgel method has
40 attracted much attention due to its inherent advantages of low processing temperature and homogenous

41 reactant distribution. The products obtained by this method exhibit high crystalline quality, narrow size
42 distribution, and uniform shape [5]. The effect of rare-earth ions inclusion into the ferrite spinel

43 structure has been reported in many literatures, however little has been reported on the effect of
44 calcination temperature on dielectric and magnetic properties. Rashad et al, [6] indicated the change in

45 the magnetic properties of samarium substituted $CoFe_2O_4$ synthesized by citrate precursor method and
46 the results revealed that the saturation magnetization and coercivity are decreased with the addition of

47 Sm^{3+} ions. Peng et al. [7] have reported an increase in crystallite size of cobalt ferrite nanoparticles by
48 the doping of gadolinium. Guo et al, [8] have reported that the substitution of Sm^{3+} in $NiFe_2O_4$

49 increases the lattice parameter and reduces the crystallite size of the materials. Tahar et al, [9] have
50 investigated the effect of Sm^{3+} and Gd^{3+} substitution on the magnetic properties of cobalt ferrite

51 synthesized by forced hydrolysis in polyol and reported that particle size increased slightly with rare
52 earth substitution.

53 In this work we investigated the effect of temperature on structural, magnetic, and dielectric properties
54 of CoFe_2O_4 nanoparticles synthesized via coprecipitation method.

55

56 **Experimental**

57 *Synthesis*

58 Required amount of iron nitrate and cobalt nitrate were dissolved in 100 ml of distilled water at room
59 temperature and stirred for 15 min continuously. During constant stirring, 100 ml of ammonia solution
60 was added in drops form. The droppings were done so as to get a solution with pH about 12. The
61 mixture solution/precipitate were dried in an oven at $80 - 100\text{ }^\circ\text{C}$ for 48 hrs. The obtained dry
62 powder were then calcined at in a furnace at $600\text{ }^\circ\text{C}$ and $900\text{ }^\circ\text{C}$ for 2 hrs. The annealed samples were
63 allowed to cool naturally to room temperature.

64 *Measurement*

65 X-ray diffraction (XRD) of the prepared sample were recorded in a Phillips diffractometer equipped
66 with a $\text{CuK}\alpha$ monochromator. The indentification of the crystalline phases present in the samples were
67 achieved using the XRD profiles. Transmission Electron Microscope (TEM) JEOL JEM 1220 was used
68 to explore the sample morphology and its particle size distribution. The room temperature infrared
69 spectra of nanopowders were recorded using a Fourier Transform Infrared Spectrophotometer Perkin
70 Elmer. The dispersing of the samples were observed in the range from 380 to 4000 cm^{-1} . The
71 temperature and field dependence of magnetization were carried out in vibrating sample magnetometer
72 (VSM). While dielectric measurement were carried out using open ended coaxial probe via Agilent HP
73 85072.

74

75 **Results and discussion**

76 ***XRD analysis***

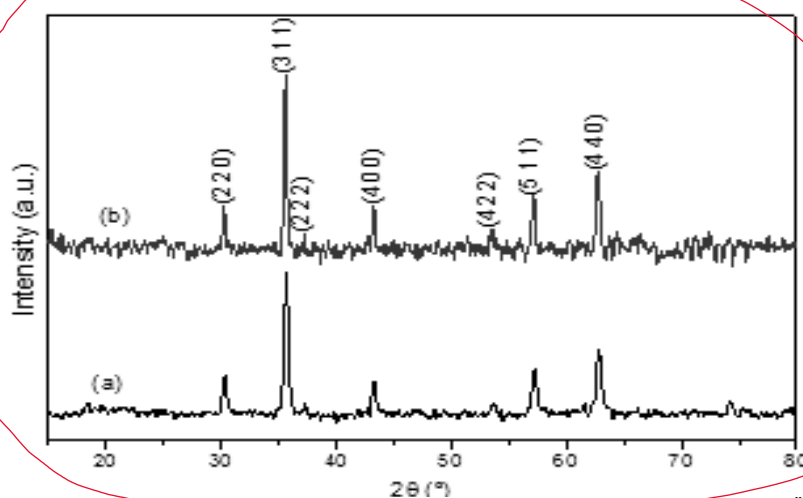
77 X- ray diffraction study of both samples confirmed the formation of single phase cubic spinel structure.

78 The single phase spinel ferrite obtained by high temperature calcination at 900 °C is in agreement with
79 the standard JCPDS data reference (JCPDS: 22-1086).

80 The micrograph of the CoFe₂O₄ sintered sample at 600 °C and 900 °C are presented in Fig. 1. The
81 average crystallite sizes were calculated by Scherer’s equation (Eq.(1)) from the intensity of reflection
82 of the spinel structure’s of the (311) plane. The equation of Scherrer is given as [10];

$$D = \frac{k\lambda}{\beta \cos\theta} \quad (1)$$

83 where k is a constant equal to 0.9, λ is the wavelength of the X-ray radiation (all diffraction patterns
84 shown in this paper were performed with CuK α radiation), θ is the diffraction angle, and β is the full
85 width half maximum (FWHM).



IF POSSIBLE
INCREASE
THE FIGURES
RESOLUTION.

86 **Figure 1: XRD pattern of cobalt ferrite nanoparticles calcined at (a) 600 °C and (b) 900 °C**

87
88
89 The lattice parameters have been computed using the d-spacing values and the respective (hkl)
90 parameters from the classical formula given in Eq.(2) [10].

$$a = \frac{\lambda[h^2 + k^2 + l^2]^{1/2}}{2\sin\theta} \quad (2)$$

91 Calculation showed that the crystallite size and lattice parameter of the powder were found to 49.8nm
92 and 8.343Å for 600 °C and 67.7 nm and 8.362Å for the 900 °C sintered sample. This finding indicated
93 that the synthesized powders had nano size crystallites and that the sintering temperature caused the
94 sample to increase in the crystallite size. In addition, the sintering temperature also led to a slight
95 increase of 0.019Å in the lattice parameter. This is attributed to the heat coupling in the sample at
96 higher temperature allowing the diffusion of metals into their octahedral sites [10].

97 The sharp increase in crystallinity of the sample is attributed to calcination **temperature** as observed for
98 the 900 °C heating.

99 ***TEM measurement***

100 Figure 2 shows the TEM images of the **prepared** Cobalt ferrite nanoparticles after annealing with
101 temperatures of 600 °C and 900 °C respectively. The particles in both cases are spherical and exhibit a
102 homogeneous distribution, especially at higher lower temperature. The average sizes of the
103 nanoparticles were found to be 43.5 nm and 62.5 nm for the 600 °C and 900 °C respectively. The result
104 obtained for the average particle size distribution were in agreement with the values obtained using the
105 XRD spectra. An increase of particle size with increasing annealing indicated that when temperature
106 increases, more metal ions are produce which in turn increases the particle sizes. This increment in
107 number of ions and particle size is supports the enhancement of the intensity of absorption as shown in
108 the FTIR spectra for the 900 °C annealed sample. It important to note that tiny amount of
109 agglomeration is observed at higher temperature due to growing distribution of particle size. A
110 summary of properties of the prepared sample is tabulated in Table 1.

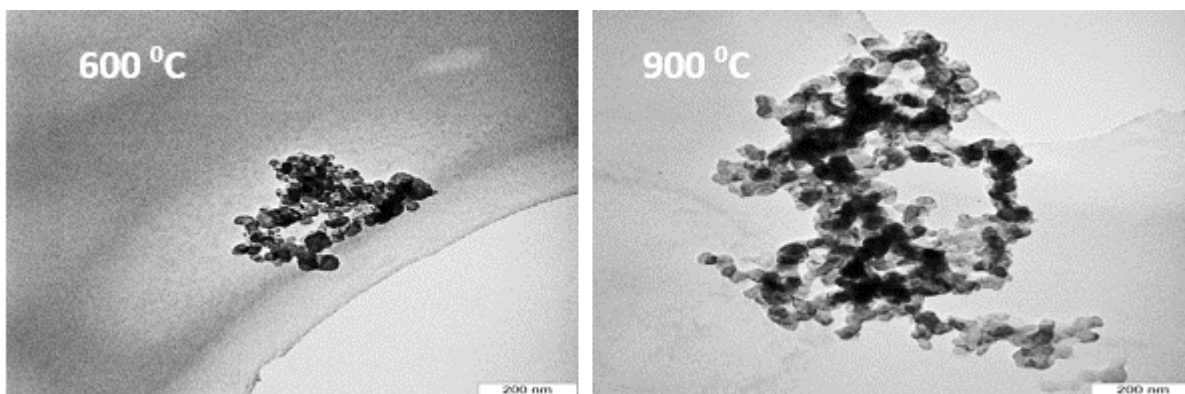


Figure 2: TEM images of cobalt ferrite nanoparticles calcined at 600 °C and 900 °C

Table 1. Magnetic parameters of cobalt ferrite

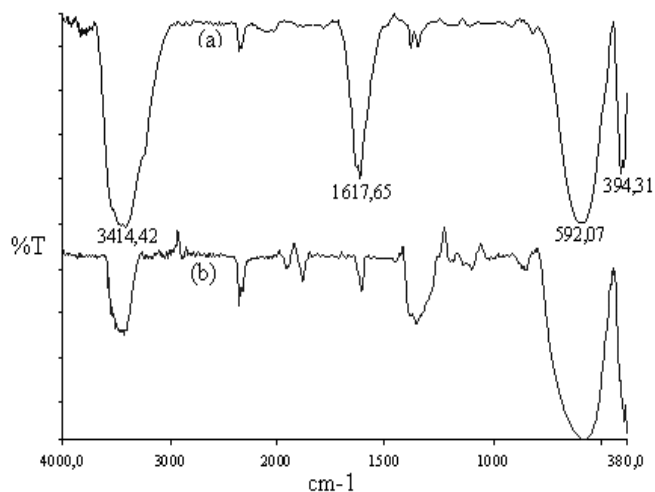
Compound	T _{calc} (°C)	a (Å)	d (nm)	H _C (Oe)	M _r (μ _B /mol)	M _s (μ _B /mol)
CoFe ₂ O ₄	600	8.343	43.5	12,405	2,819	3,349
				696	937	2,987
	900	8.362	62.5	10,640	3,080	3,569
				720	1,048	3,294

111
112
113
114

115

116 **FTIR Spectroscopy**

117 Careful observation on the FTIR spectra shown in figure 3 shows an absorption peak at 592cm⁻¹
 118 corresponding to intrinsic stretching vibrations of metal at the tetrahedral site, whereas the v₂-lowest
 119 band, observed in the range of 400–300cm⁻¹, is due to the octahedral–metal stretching [11]. Co²⁺ ions
 120 usually occupy octahedral-site, while Fe³⁺ ions has the tendency to occupy both octahedral and
 121 tetrahedral sites [12]. Further observations shows strong absorptions peaks at 3414 and 1617cm⁻¹
 122 wavelengths.



123 **Figure 3: FTIR spectra of cobalt ferrite nanoparticles calcined at (a) 600 °C and (b) 900 °C**

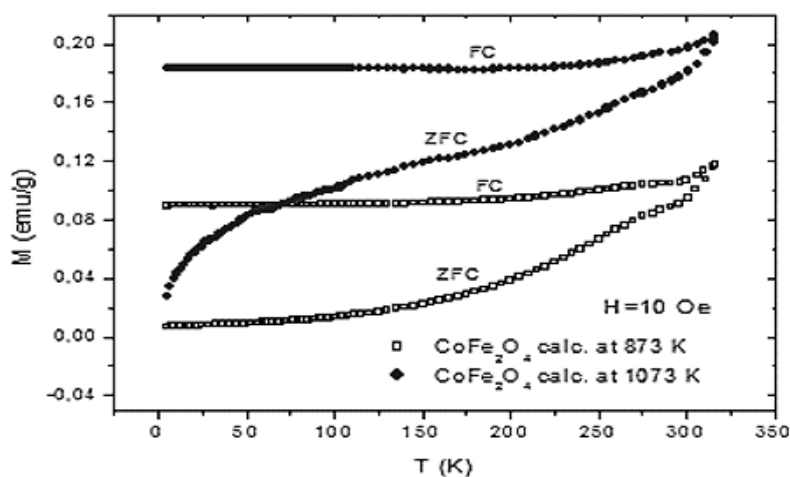
124
125
126 ***Magnetic measurement***

127 Figure 4, represents the ZFC and FC curves of magnetization of both temperatures. Both ZFC and FC
128 magnetization decreases by increasing the temperature. At low temperatures in the presence of a
129 magnetic field (FC), the magnetization direction of each particle is frozen in the field direction. While
130 the ZFC magnetization is below the magnitude for FC. Both ZFC and FC magnetization is increasing
131 by increasing the temperature. However, at higher calcination temperature, the magnetization in both
132 cases is lower than that compared at low temperature. In both cases, the ZFC and FC curves are
133 **seperated** given an indication that there is a non-equilibrium magnetization below the separation
134 temperature. For the ZFC case, the seperation represents the irreversibility temperature, (T_{irr}).

135 In general, T_c represents the blocking-unblocking process of the particles magnetic moment when
136 thermal energy is changed [13]. As the relaxation time of a magnetic particle decreases with increasing
137 temperature, below a certain characteristic temperature called the blocking temperature (T_B) the
138 particles moment remains blocked with respect to the time scale of the experiment. The difference
139 between T_B and T_{irr} corresponds to the width of the blocking temperature distribution which gives an
140 indication of the narrowness of the **anisotrop yenergy** barrier distribution of the particles [13,14].

141 Below the T_{irr} , the ZFC and FC curves significantly diverge and the sample is in the ferromagnetic

142 state. The divergence in the ZFC–FC magnetization curves below T_B is attributed to the existence of
 143 magnetic anisotropy barriers [14].

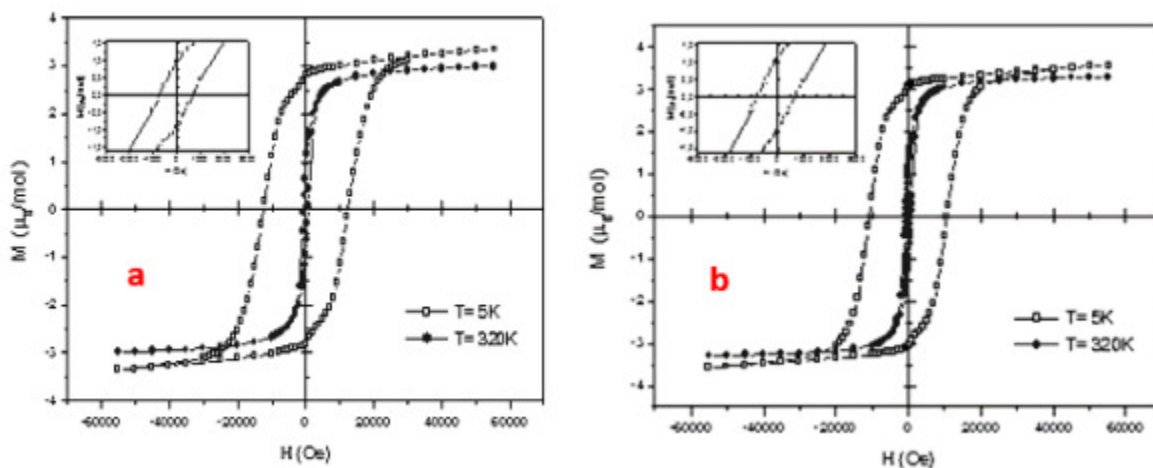


144

145 **Figure 4: Temperature dependent magnetizations of sample**

146

147 This behavior is confirmed by the isothermal magnetization curves obtained at 5 K and 320 K shown in
 148 Fig. 5. These results are in agreement with analysis obtained for the ZFC/FC discussed in Figure 4. The
 149 saturation temperature, coercive was highest at 5 K for both annealing temperatures as shown in Table
 150 1. Whilst the magnetic hysteresis at 5K showed very large hysteresis with coercive fields of 12405 and
 151 10640 Oe for 600 °C and 900 °C annealing respectively.



152

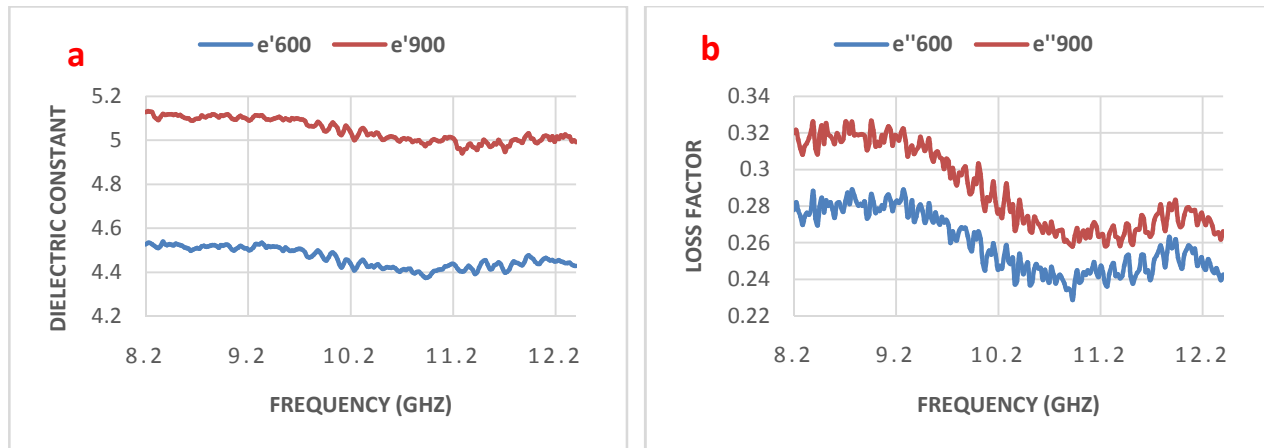
153 **Figure 5: Hysteresis loops of the samples at (a) 600 °C and (b) 900 °C**

154

155 Further observation showed that in Fig. 5 the coercivity of the nanoparticles decreases as the
156 temperature increases toward the blocking temperature. The inserts in Fig. 5 show the part of the $M(H)$
157 loops in the region of small applied field. The saturation magnetization is dependent on the thermal
158 treatment where saturation magnetization obtained were, $M_S = 3.349 \mu_B/\text{mol}$ for sample calcined at 600
159 $^{\circ}\text{C}$ and $M_S = 3.569 \mu_B/\text{mol}$ for sample calcined at 900 $^{\circ}\text{C}$ at 5K. In order to verify the obtained
160 inversion degree in the cobalt ferrite prepared in this work, we used The highest saturation
161 magnetization: $M_S = 3.569 \mu_B/\text{mol}$ was used to verify inversion degree obtained in this work. The
162 inversion degree obtained was $\lambda = 0.85$.

163 *Dielectric measurement*

164 Open ended coaxial probe (Agilent 85702B) was used in the measurement of complex permittivity of
165 both samples. The measurement was carried out at microwave frequency (8.2 GHz to 12.4 GHz).
166 Careful observation on Figure 6(a) shows that dielectric constant decreases with the increase of
167 frequency in both samples. The dependence of dielectric constant on frequency can be explained using
168 interfacial polarization as predicted by Maxwell-Wagner [15]. It is expected that the dielectric structure
169 of a ferrite is made up of a conductive layer that consists of large ferrite grains and other grain
170 boundaries that are poor conductors. Polarization is mainly due to electron exchange between Fe^{+2} and
171 Fe^{+3} in the direction of applied field. Measurement result showed that the mean directly constant were
172 4.46 and 5.05 for the 600 $^{\circ}\text{C}$ and 900 $^{\circ}\text{C}$ annealed samples respectively.



173

174

Figure 6: Complex permittivity of samples annealed at 600 °C and 900 °C

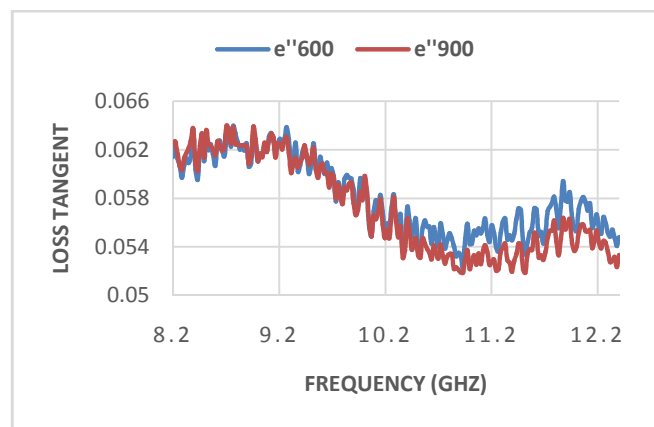
175

176

177

178

As shown in figure 6(b), the large value of loss factor at lower frequency might be attributed to the dominant species like Fe^{+2} ions, oxygen vacancies, grain boundary defects, etc. The loss factor at high frequency are due to particles which have low resistivity. The mean loss factor obtained for both samples are 0.26 and 0.29 for the 600 °C and 900 °C calcinations respectively.



179

180

Figure 7: Loss tangent of samples at annealed at 600 °C and 900 °C

181

182

183

184

185

Figure 7 depicts the loss factor obtained from the ratio of loss factor to the dielectric constant. The loss tangent ($\tan\delta$) decreases with the increase of frequency and then begins to stagnate at higher frequencies for both samples. The mean magnitude of the loss tangent obtained are 0.058 and 0.057 for the 600 °C and 900 °C calcinations respectively. This results indicates that the 600 °C annealed sample would absorb higher than the 900 °C annealed sample. The loss ($\tan\delta$) depends on factors, such as

186 material stoichiometry, Fe^{+2} content and material dispersion, which in turn depends on the composition
187 and synthesis methods. The decrease in loss tangent with frequency may be attributed to the Maxwell-
188 Wagner polarization and conduction mechanism in ferrites [16].

189

190 **Conclusions**

191 The thermal heat caused an increase in the average crystallite size, magnetization and the coercive field
192 of the sample. Similarly, infrared spectroscopy studies confirms the presence of metal oxide in the
193 prepared nanoparticles. The main characteristic of the field cooled (FC) and zero field cooled (ZFC)
194 curves is its irreversibility below room temperature suggesting the presence of a superparamagnetic
195 behavior. In addition, the magnetic properties exhibit some dependence on the calcination temperature.

196 The M_S values increases with the increase of calcination temperature whilst the maximum value of H_C
197 is about 12405 Oe which is much higher than the coercivity of bulk material. The increase in the
198 value of lattice parameter with increase in temperature suggests the expansion of the unit cell.

↳ HOW MUCH HIGHER?

199 Crystallinity and the crystallite size are observed to increase with increase in temperature. The average
200 particle sizes estimated from TEM micrographs were 43.5 nm for sample calcined at 600 °C and 62.5
201 nm for sample calcined at 900 °C.

202

203 **References**

204 [1] Köseoğlu, Y., Olewi, M. I. O., Yilgin, R., & Koçbay, A. N. (2012). Effect of chromium addition on
205 the structural, morphological and magnetic properties of nano-crystalline cobalt ferrite
206 system. *Ceramics International*, 38(8), 6671-6676.

207 [2] Carta, D., Casula, M. F., Falqui, A., Loche, D., Mountjoy, G., Sangregorio, C., & Corrias, A.
208 (2009). A structural and magnetic investigation of the inversion degree in ferrite nanocrystals MFe_2O_4
209 (M= Mn, Co, Ni). *The Journal of Physical Chemistry C*, 113(20), 8606-8615.

- 210 [3] Xavier, S., Thankachan, S., Jacob, B. P., & Mohammed, E. M. (2013). Effect of Samarium
211 Substitution on the Structural and Magnetic Properties of Nanocrystalline Cobalt Ferrite. *Journal of*
212 *Nanoscience*, Vol. 2013. <http://dx.doi.org/10.1155/2013/524380>
- 213 [4] Raj, K., Moskowitz, B., & Casciari, R. (1995). Advances in ferrofluid technology. *Journal of*
214 *magnetism and magnetic materials*, 149(1), 174-180.
- 215 [5] Kim, D. K., Zhang, Y., Kehr, J., Klason, T., Bjelke, B., & Muhammed, M. (2001). Characterization
216 and MRI study of surfactant-coated superparamagnetic nanoparticles administered into the rat
217 brain. *Journal of Magnetism and Magnetic Materials*, 225(1), 256-261.
- 218 [6] Rashad, M. M., Mohamed, R. M., & El-Shall, H. (2008). Magnetic properties of nanocrystalline Sm-
219 substituted CoFe₂O₄ synthesized by citrate precursor method. *journal of materials processing*
220 *technology*, 198(1), 139-146.
- 221 [7] Peng, J., Hojamberdiev, M., Xu, Y., Cao, B., Wang, J., & Wu, H. (2011). Hydrothermal synthesis
222 and magnetic properties of gadolinium-doped CoFe₂O₄ nanoparticles. *Journal of Magnetism and*
223 *Magnetic Materials*, 323(1), 133-137.
- 224 [8] Guo, L., Shen, X., Meng, X., & Feng, Y. (2010). Effect of Sm³⁺ ions doping on structure and
225 magnetic properties of nanocrystalline NiFe₂O₄ fibers. *Journal of Alloys and Compounds*, 490(1),
226 301-306.
- 227 [9] Tahar, L. B., Smiri, L. S., Artus, M., Joudrier, A. L., Herbst, F., Vaulay, M. J., ... & Fiévet, F.
228 (2007). Characterization and magnetic properties of Sm- and Gd-substituted CoFe₂O₄ nanoparticles
229 prepared by forced hydrolysis in polyol. *Materials Research Bulletin*, 42(11), 1888-1896.
- 230 [10] Yakubu, A., Abbas, Z., Hashim, M. and Fahad, A. (2015). Effect of Sintering Temperature on
231 Co_{0.5}Zn_{0.5}Fe₂O₄ Nano-Particles Evolution and Particle Size Distribution. *Advances in Nanoparticles*,
232 **4**, 37-44. <http://dx.doi.org/10.4236/anp.2015.42005>
- 233 [11] Hafner, S. (1961). The absorption of some metal oxides with spinel structure, *Zeitschrift Fur*

234 *Kristallographie*, 115, 331–358.

235 [12] Yoon, S. J., Lee, S. H., Kim, K. H., & Ahn, K. S. (2002). Electrical and magnetic properties of
236 spinel $ZnCr_{2-x}Fe_xO_4$ ($0 \leq x \leq 1.0$). *Materials chemistry and physics*, 73(2), 330-334.

237 [13] Sertkol, M., Köseoğlu, Y., Baykal, A., Kavas, H., & Başaran, A. C. (2009). Synthesis and
238 magnetic characterization of $Zn_{0.6}Ni_{0.4}Fe_2O_4$ nanoparticles via a polyethylene glycol-assisted
239 hydrothermal route. *Journal of Magnetism and Magnetic Materials*, 321(3), 157-162

240 [14] Nathani, H., & Misra, R. D. K. (2004). Surface effects on the magnetic behavior of nanocrystalline
241 nickel ferrites and nickel ferrite-polymer nanocomposites. *Materials Science and Engineering:*
242 *B*, 113(3), 228-235.

243 [15] Wagner, K. W. (1913). The theory of incomplete dielectricity. *Annals of Physics*, 40, 817.

244 [16] Kumar, H., Srivastava, R. C., Negi, P., Agrawal, H. M., & Asokan, K. (2013). Dielectric
245 Behaviour of Cobalt Ferrite Nanoparticles. *International Journal of Electrical and Electronics*
246 *Engineering*, 2, 59-66.

247